Constrained Gaussian Condensation Filter for Cooperative Target Tracking

Cheng Xu, *Member, IEEE*, Hang Wu, and Shihong Duan

***Abstract*—Real-time high-precision navigation has many applications, such as pedestrian navigation, emergency rescue, and vehicle networks. In practice, the measurement models are often nonlinear, and sequential Bayesian filters, such as Kalman and particle filter, suffer from accumulative errors, which cannot provide long-time high-precision services for localization. To solve arbitrary noise distribution, this article proposes a Gaussian condensation filter (GCF) algorithm to achieve high-precision localization in a non-Gaussian noise environment. To this end, we proposed an error-ellipse resampling (EER)-based GCF (EER-GCF), which establishes error ellipses with different confidence probabilities and implements a resampling algorithm based on the sampling points' geometrical positions. Furthermore, a cooperative EER-based GCF (CEER-GCF) is proposed to enhance information fusion in the multitarget network. This study accomplishes cooperative tracking based on spatial–temporal constraints to enhance error correction. The experimental results show that CEER-GCF can effectively eliminate the accumulative error and optimize state estimation, which outperforms state of the arts, such as unscented Kalman filter and particle filter.**

***Index Terms*—Cooperative tracking, error-ellipse resampling (EER), Gaussian mixture distribution, location aware, spatial–temporal constraints.**

I. Introduction

NOWADAYS, real-time and high-accuracy localization has been considered for many civil and military applications, such as pedestrian navigation [1], emergency rescues [2], and intelligent vehicles [3]. The global navigation satellite system (GNSS) is sufficient to provide qualified accuracy positioning support for substantial outdoor positioning applications [3]. However, in some harsh environments, including densely constructed urban areas, underground, forests, and canyons, there is a high probability of GNSS signals being blocked or lost, which makes GNSS scarcely meet the practical demands. Wireless positioning techniques, such as ultra wideband (UWB) based on time-of-arrival (TOA) distance measurements [4], are widely adopted in areas that GNSS cannot cover. However, in most conditions, it requires the predeployment of base stations [5]. The inertial navigation system (INS) that utilizes an inertial measurement unit (IMU) is self-contained and could infer its position from sequential data without any additional infrastructure [6]. Unfortunately, INS is constrained to a large extent by the cumulative error problem [7], so that it cannot provide a long-term high-precision estimation.

Correspondingly, existing methods generally consider fusion and cooperative methods [8], [9]. Zihajehzadeh and Park [8] put forward a method with IMU/TOA fusion, which combined the characteristics of instantaneous high-precision measurement of IMU and nonaccumulative error of TOA. However, external beacons are still required, which is unsuitable for extensive area tracking or collaborative scenarios. Xu *et al.* [9] also provided a reliable implementation with IMU/TOA fusion for human motion tracking. They realize long-term and large-distance requirements by mounting several sensing nodes onto human joints. Nevertheless, it is not easy to generalize to general target tracking applications due to its strict model. Filtering methods are also widely considered to solve cooperative fusion problems. Kalman-like filters have been widely applied for many important problems. The Kalman filter [4], [10] is the most widely adopted Bayesian estimator to minimize the variance of the estimation error. It is a recursive algorithm that uses a model of dynamics and sensor measurements to obtain an estimation of the state vector. However, it strictly requires the system model to be linear and assumes the noise to be Gaussian white noise, which greatly limits its application in complex systems and practical environments. Extended Kalman filter (EKF) [11], [12] is considered with linearizing the nonlinear state model, but it is only applicable to weak linear systems. However, due to the selection of linearization points and the abandonment of higher order terms, there will be an inevitable linearization error. To solve this, You *et al.* [13] proposed an unscented Kalman filter (UKF) to realize UWB and IMU fusion in indoor localization of quad-rotors. It can approximate the posterior distribution based on sampling points, but the non-Gaussian noise problem remains unsolved.

Most of the existing IMU/TOA fusion literature mainly considered the ambient noise as Gaussian, such as [7] and [14]–[17]. However, in certain conditions, such as suburban and urban environments, due to manufactured

Manuscript received January 26, 2021; revised June 2, 2021; accepted June 7, 2021. Date of publication June 10, 2021; date of current version January 24, 2022. This work was supported in part by the China National Postdoctoral Program for Innovative Talents under Grant BX20190033; in part by the Guangdong Basic and Applied Basic Research Foundation under Grant 2019A1515110325; in part by the Project funded by the China Postdoctoral Science Foundation under Grant 2020M670135; in part by the Postdoctor Research Foundation of Shunde Graduate School of University of Science and Technology Beijing under Grant 2020BH001; and in part by the Fundamental Research Funds for the Central Universities under Grant 06500127. *(Cheng Xu and Hang Wu are co-first authors.) (Corresponding author: Cheng Xu.)*

The authors are with the School of Computer and Communication Engineering, University of Science and Technology Beijing, Beijing 100083, China, also with the Shunde Graduate School, University of Science and Technology Beijing, Foshan 528300, China, and also with the Beijing Laboratory of Knowledge Engineering for Materials Science, Beijing 100083, China (e-mail: xucheng@ustb.edu.cn; wuhang@xs.ustb.edu.cn; duansh@ustb.edu.cn).

Digital Object Identifier 10.1109/JIOT.2021.3088297

environmental factors, different sensor measurements often show various distribution characteristics, most of which are usually non-Gaussian. TOA distance ranging is easily influenced by the multipath and nonline of sight (NLOS) factors. Typically, ranging errors can be modeled as a Gaussian distribution in the line of sight (LOS) scenarios [18]. In the NLOS scenarios, ranging errors can be modeled as Gaussian distribution [7], log normal [19], or other non-Gaussian distributions [20], [21]. Besides, IMU measurement noise is often non-Gaussian and random with significant impulse characteristics [22]. α-stable distribution [20], [23] and Student-t distribution [24]–[26] are often considered in noise modeling of inertial sensors, and it is generally believed that IMU's noise is non-Gaussian and exhibits different characteristics in various environments.

Therefore, the Gaussian assumption, to some extent, does not conform to the real-world noise situation. There are still challenges in realizing a fusion positioning solution for arbitrary noise distribution. Wang *et al.* [15] proposed the particle filter (PF) based on Monte Carlo sampling, which uses the average value of a set of weighted particles to estimate the mean and covariance of the state, and approximates the posterior distribution in the region containing the significance probability. However, in the process of resampling, it faces the problem of particle degradation and depletion [27]. In addition, for high-dimensional problems, high complexity is usually inevitable [28].

The cooperative optimization technique is considered to suppress the impact of accumulative errors in autonomous navigation and positioning. In self-organizing and highly dynamic scenarios, the cooperative technique can fuse the perception information collected by individuals to realize the information gain between target nodes. Specifically, a target node obtains location from an inertial measurement device in a cooperative network and generates autonomous ranging information with others. Based on this mutual information, they coordinate with each other to complete an optimized estimation of target positioning [29]. With inertial measurement sensors and ranging sensors embedded, the mobile nodes can realize multitarget cooperative positioning based on the inertial measurement and spatial distance measurement [7]. When we consider static space optimization, we pay attention to the influence of space measurement at the current moment on the state estimation. The state constraints can be obtained based on the distance measurement among the nodes. Nilsson *et al.* [30] proposed a cooperative positioning technique using spatial location information to achieve the optimization of the multitarget location tracking. However, these distance fusion methods require external base stations, and the wireless signal is prone to NLOS occlusion, which may cause large errors.

In this perspective, we show how to include constraints in the part of the Gaussian condensation filter. With error-ellipse and distance constraints applied to the estimation process of the temporal filter, the estimated state is closer to the real position. In terms of uncertainty quantification, Cramér–Rao lower bound (CRLB) is a well-adopted tool in the existing literature to quantify the measurement uncertainty [7], [31]. In this current study, we detailed the derivation

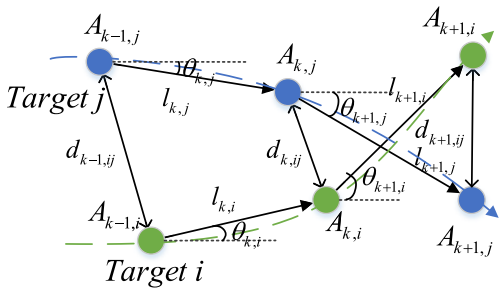

Fig. 1. Example trajectory of walking target nodes: step size l_k and heading angle θ_k can be obtained by an IMU, and $d_{k,ij}$ can be obtained by range measurements with respect to other nodes.

of constrained sequential bound of cooperative networks. Moreover, to evaluate the performance of different methods, we also derived the posterior CRLB (PCRLB) for this problem. Simulation results confirm these bounds. In summary, the main contributions of this article are threefold.

1) A Gaussian condensation filter (GCF) method is proposed to effectively handle the arbitrary noise distribution, aiming at the non-Gaussian noise problem of the target tracking. We adopted a Gaussian mixture model to approximate the true posterior probability distribution.
2) To conquer the cumulative error problem of target tracking, we utilized the error-ellipse resampling (EER) method to realize resampling based on the sample points' geometric positions. A 3σ − and $-\sigma$ uncertainty discriminate criterion is established to construct the inner and outer error-ellipses centered at IMU's initial estimation. With duplicating and deleting the sample points, the impact of accumulative errors is effectively suppressed.
3) Furthermore, a spatial-constrained GCF is proposed to improve the information fusion in the cooperative network effectively. By using the mutual information constraints between target nodes, the tracking positions could be cooperatively optimized. Thereby, the state estimation of the target node is improved.

The remainder of this article is organized as follows. Section II gives the symbolic explanation, related definitions, and problem description. Section III proposes a multitarget cooperative GCF (CGCF) algorithm, which describes the EER algorithm and the process of cooperative constraint optimization. Section IV analyzes the theoretical performance of cooperative target tracking. Section V details the experiment results. Finally, conclusion is drawn in Section VI.

II. Problem Definition

In this section, we investigate the filtering problem for navigation in harsh environments as a case study. We consider a two-dimensional scenario in which a target node could obtain internode distance ranges to the others and intranode inertial measurements from IMU. In the following, we, respectively, describe the dynamic and measurement model.

A. Dynamic Model

Fig. 1 illustrates the random walk model [15] of target nodes. Define a set $\Omega = \{1, 2, \ldots, M\}$ with M mobile targets,

whose position is unknown. The state vector $X_{k,i} \in \mathbb{R}^2$ of the ith moving target at time k is indicated, where the measured coordinate vector $A_{k,i} = [x_{k,i}, y_{k,i}]^T$ and the velocity vector is $V_{k,i}$. Therefore, the state parameter X_k at time k can be expressed as

$$X_k = \left[A_{k,1:M}, V_{k,1:M}\right]^T. \tag{1}$$

Generally, the random walk model can be modeled as a Gaussian Markov process. The state X_k of the ith moving target at time k transfers to the state X_{k+1} at time $k+1$. The state transition equation is expressed as

$$X_{k+1,i} = \begin{bmatrix} x_{k+1,i} \\ y_{k+1,i} \\ V_{k+1,i} \end{bmatrix} = F \begin{bmatrix} x_{k,i} \\ y_{k,i} \\ V_{k,i} \end{bmatrix} + G\upsilon_k \tag{2}$$

where

$$F = \begin{bmatrix} 1 & 0 & \Delta t \cos\hat{\theta}_{k,i} \\ 0 & 1 & \Delta t \sin\hat{\theta}_{k,i} \\ 0 & 0 & 1 \end{bmatrix} \text{ and } G = \Delta t \begin{bmatrix} \Delta t/2 \cos\hat{\theta}_{k,i} \\ \Delta t/2 \sin\hat{\theta}_{k,i} \\ 1 \end{bmatrix}$$

represent state transition matrices. The variable Δt is the sampling interval, and $\theta_{k,i}$ is the horizontal angle of the ith target node at time k. Commonly, a dynamic error is modeled as a zero-mean Gaussian variable [32]. υ_k is the dynamic noise, which obeys Gaussian distribution with a mean of 0 and a covariance of γ^2, namely, $\upsilon_k \sim N(0, \gamma^2)$. Thus, the dynamic model for the state vector in navigation can be considered as linear and Gaussian without loss of generality.

B. Measurement Model

In localization and navigation problems, parameters of the random walk model are generally composed of step and angle information. With the accelerometer measurements of the IMU sensor, the ith target node's step size estimate is

$$\hat{l}_{k,i} = l_{k,i} + \eta_{1,k} \tag{3}$$

where $l_{k,i}$ is the actual distance displacement between the positions of time k and $k+1$, i.e., step size, which could be represented as

$$l_{k,i} = \sqrt{\left(x_{k+1,i} - x_{k,i}\right)^2 + \left(y_{k+1,i} - y_{k,i}\right)^2} \tag{4}$$

and $\eta_{1,k}$ is the step error and could fit for the arbitrary distribution, namely, Gaussian and non-Gaussian in various conditions. Therefore, the vector $\hat{l} = [\hat{l}_{k,1}, \hat{l}_{k,2}, \ldots, \hat{l}_{k,M}]^T$ shows the step size information at time k. With the gyroscope measurements of the IMU sensor, the ith target node's horizontal angle estimate is

$$\hat{\theta}_{k,i} = \theta_{k,i} + \eta_{2,k} \tag{5}$$

where $\theta_{k,i}$ is the actual horizontal angle, i.e.,

$$\theta_{k,i} = \arctan\frac{y_{k+1,i} - y_{k,i}}{x_{k+1,i} - x_{k,i}} \tag{6}$$

and $\eta_{k,i}$ is the horizontal angle error and obeys the arbitrary distribution, namely, Gaussian and non-Gaussian in various conditions. Therefore, the vector $\hat{\theta}_k = [\hat{\theta}_{k,1}, \hat{\theta}_{k,2}, \ldots, \hat{\theta}_{k,M}]^T$ shows the horizontal angle at time k. The distance between the ith and the jth target node is estimated as

$$\hat{d}_{k,ij} = d_{k,ij} + \eta_{3,k} \tag{7}$$

where $d_{k,ij}$ is the actual distance at time k, i.e.,

$$d_{k,ij} = \sqrt{\left(x_{k,i} - x_{k,j}\right)^2 + \left(y_{k,i} - y_{k,j}\right)^2} \tag{8}$$

and $\eta_{3,k}$ is the distance error and obeys the arbitrary distribution, namely Gaussian and non-Gaussian in various conditions. Therefore, the vector $S_k = \{\hat{d}_{k,ij} \mid j \in \{1, \ldots, M\} \setminus \{i\}\}$ shows the distance between the target node and others at time k. For simplicity, we define $Z_k = [\hat{l}_k, \hat{\theta}_k]$ as the inertial measurements of M target nodes. Similarly, S_k is for the distance ranging measurements.

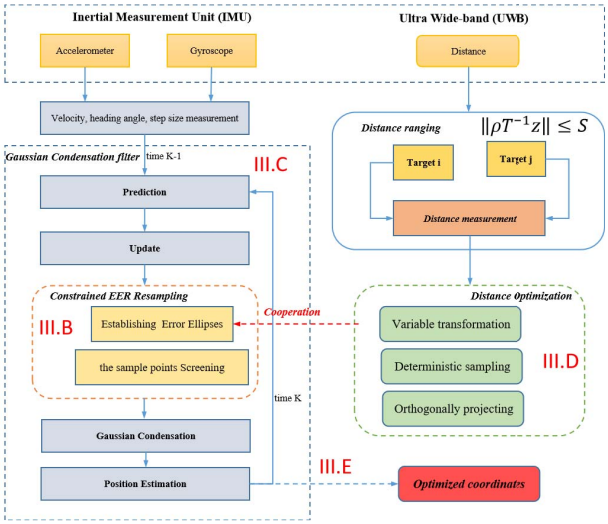

Fig. 2. IMU consists of the accelerometer and the gyroscope, and both will obtain the measurement at each moment. These values are used as the initial input for GCF. The UWB sensor provides the essential distance information, which ensures the procedure of distance optimization for constrained EER in the cooperative stage.

III. Cooperative Gaussian Condensation Filter

This section first details the GCF to handle non-Gaussian noise in the measurement model under nonideal conditions. On this basis, we optimize the sampling points with the use of their geometric position. Then, we introduce an EER-based GCF (EER-GCF) algorithm to accomplish the temporal state estimation of the target node. After that, we introduce constraint optimization based on spatial distance. Finally, a CGCF is established to realize multitarget cooperation with the consideration of spatial–temporal constraints. Fig. 2 describes the flow of the cooperative-constrained Gaussian condensation filter.

A. Gaussian Condensation Filter

The Gaussian condensation filter [33] recursively generates the posterior probability density function (PDF) of the target state. Fig. 3 illustrates the key ideas of GCF. In the *prediction* step, the prior PDF can be calculated from the posterior distribution of the previous moment. In the *update* step,

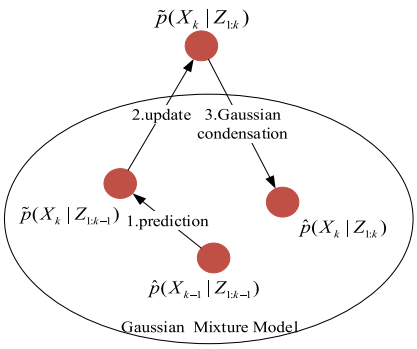

Fig. 3. Illustration of the GCF in three steps: 1) *prediction*; 2) *update*; and 3) *Gaussian condensation*.

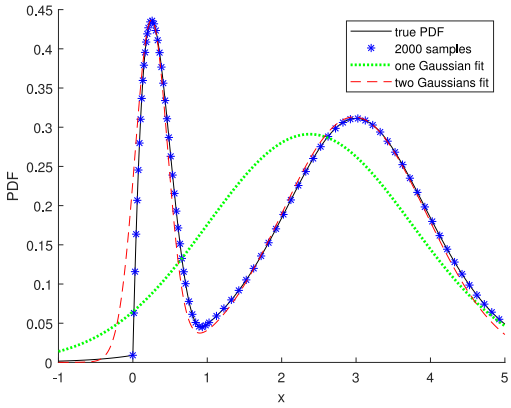

Fig. 4. PDF of a mixture of one beta and one t-student distribution, as well as the fitting results with 2000 samples and two kinds of approximation, respectively, one and two Gaussian kernel fitting.

the posterior PDF is updated by a new set of measured values. In the *Gaussian condensation* step, due to the nonlinearity of the measurement model, *a posteriori* PDF is approximated as the Gaussian mixture model. Then, the estimated state is projected back into the Gaussian mixture model.

1) Prediction: It is assumed that the state transition process obeys the first-order Markov model, namely, $p(X_k|X_{1:k-1}) = p(X_k|X_{k-1})$. At time k, *a priori* probability distribution $p(X_k|Z_{1:k-1})$ can be calculated by the integration of the product of $p(X_k|X_{k-1})$ with $p(X_{k-1}|Z_{1:k-1})$. However, the integral is extremely complicated in non-Gaussian systems. It can only be efficiently solved when the involved functions are Gaussian or sums of deltas, which are the intrinsic properties of Kalman-like and PFs. Moreover, according to the central limit theorem, any statistical distribution could be approximated by a Gaussian mixture, whose number of components is much smaller than that of using a mixture of deltas [34]. As the dynamic models are Gaussian and linear with a wide generality, the prediction step could be easily computed in a closed form. Therefore, in this study, we consider that the state equation is linear but the posterior distribution is a Gaussian mixture model, namely, $\hat{p}(X_{k-1}|Z_{1:k-1}) = \sum_{i=1}^{m} \alpha_i \mathcal{N}(X_{k-1}; \mu_{k-1|k-1}^{(i)}, Q_{k-1|k-1}^{(i)})$. Then, the prediction step is expressed as

$$\tilde{p}(X_k|Z_{1:k-1}) = \sum_{i=1}^{m} \alpha_i \mathcal{N}\left(X_k; \mu_{k|k-1}^{(i)}, Q_{k|k-1}^{(i)}\right) \tag{9}$$

where $\mu_{k|k-1}^{(i)} = F_k \mu_{k-1|k-1}^{(i)}$ and $Q_{k|k-1}^{(i)} = F_k Q_{k-1|k-1}^{(i)} F_k^T + \gamma^2$. m is number of Gaussian kernels and γ^2 is the covariance of dynamic noise υ_k.

2) Update: *A posteriori* PDF is updated by measurements Z_k at time k. Since the measurement model determined by the likelihood function $p(Z_k|X_k)$ is nonlinear and non-Gaussian, the updated *a posteriori* distribution $p(X_k|Z_{1:k})$ will not fall in the range of the Gaussian mixture model, as indicated in Fig. 3. Based on (9), the update step is expressed as

$$\tilde{p}(X_k|Z_{1:k}) \propto \sum_{i=1}^{m} \alpha_i \mathcal{N}\left(X_k; \mu_{k|k-1}^{(i)}, Q_{k|k-1}^{(i)}\right) p(Z_k|X_k). \tag{10}$$

3) Gaussian Condensation: For general nonlinear/non-Gaussian filters, the number of sufficient statistics characterizing the true posterior distribution increases without bound [34]. To avoid this situation, we intend to obtain a closed-form solution with the resort to approximate the posterior distribution into a Gaussian mixture model. For a given distribution p, an optimal Gaussian mixture distribution q could be derived by minimizing the Kullback–Leibler (KL)-divergence. Then, the following theorem could be used.

Theorem 1: Let $p(X)$ be the PDF of a random vector $X \in \mathbb{R}^n$ and $\lambda = (\alpha_1, \ldots, \alpha_m, \mu_1, \ldots, \mu_m, \Sigma_1, \ldots, \Sigma_m)$ be the parameters characterizing a mixture of m Gaussian distributions, namely, $q(X; \lambda) = \sum_{i=1}^{m} \alpha_i \mathcal{N}(X; \mu_i, \Sigma_i)$. If $\Phi(\lambda)$ is the KL-divergence between $p(X)$ and $q(X; \lambda)$, namely

$$\Phi(\lambda) = D_{KL}(p(X), q(X; \lambda)) = E_p\left\{\log\frac{p}{q}\right\} \tag{11}$$

then $\lambda^* = (\alpha_1^*, \ldots, \alpha_m^*, \mu_1^*, \ldots, \mu_m^*, \Sigma_1^*, \ldots, \Sigma_m^*)$ is a stationary point of Φ, where

$$q_i(X; \lambda) = \alpha_i \mathcal{N}(X; \mu_i, \Sigma_i) \tag{12}$$

$$\alpha_i = E_p\left\{\frac{q_i(X; \lambda)}{q(X; \lambda)}\right\} \tag{13}$$

$$\mu_i = \frac{E_p\left\{\frac{q_i(X;\lambda)}{q(X;\lambda)} X\right\}}{E_p\left\{\frac{q_i(X;\lambda)}{q(X;\lambda)}\right\}} \tag{14}$$

$$\Sigma_i = \frac{E_p\left\{\frac{q_i(X;\lambda)}{q(X;\lambda)} (X - \mu_i)(X - \mu_i)^T\right\}}{E_p\left\{\frac{q_i(X;\lambda)}{q(X;\lambda)}\right\}} \tag{15}$$

and $E_p(\cdot)$ indicates the expectation over a random vector p.

Proof: See the Appendix. ■

To summarize, given by a PDF $p(X)$, an approximate Gaussian mixture model could be inferred by the following steps. Given an initial solution $\lambda^0 = (\alpha_1^{(0)}, \ldots, \alpha_m^{(0)}, \mu_1^{(0)}, \ldots, \mu_m^{(0)}, \Sigma_1^{(0)}, \ldots, \Sigma_m^{(0)})$ to parameterize the Gaussian mixture $\hat{p}(X_k|Z_{1:k})$. Then, repeat the iteration $\lambda^{(j+1)} = \lambda^{(j)}$ until convergence. Fig. 4 details how we can approximate a complex statistical distribution to a Gaussian mixture one. A detailed description of GCF is shown in Algorithm 1.

Algorithm 1 GCF

Input: $\tilde{p}_k \leftarrow$ the posterior probability distribution
Output: $\{\lambda_k, \hat{p}_k\} \leftarrow$ Gaussian mixture distribution
(i) Choose a family of mixtures of Gaussian and an initial solution
$q(X, \lambda^0) = \sum_{i=1}^{m} \alpha_i^{(0)} \mathcal{N}(X, \mu_i^{(0)}, \Sigma_i^{(0)})$
$\lambda^0 = (\alpha_1^{(0)}, \cdots, \alpha_m^{(0)}, \mu_1^{(0)}, \cdots, \mu_m^{(0)}, \Sigma_1^{(0)}, \cdots, \Sigma_m^{(0)})$
(ii) $\Phi(\lambda)$ repeat until convergence the iteration
while $\lambda^{(j+1)} = \lambda^{(j)}$ **do**
  for $i \leftarrow 1, m$ **do**
    $f(X) = \frac{\alpha_i^{(l)} \mathcal{N}(X; \mu_i^{(l)}, \Sigma_i^{(l)}) \tilde{p}_k}{\sum_{i=1}^{m} \alpha_i^{(l)} \mathcal{N}(X; \mu_i^{(l)}, \Sigma_i^{(l)})} \triangleright formula(13)$
    $\alpha_i^{(l+1)} = f(X)$
    $\mu_i^{(l+1)} = \frac{sum(Xf(X))}{C} \triangleright formula(14)$
    $\Sigma_i^{(l+1)} = \frac{sum((X-\mu_i^{(l+1)})(X-\mu_i^{(l+1)})^T f(X))}{C}$
  end for
end while
(iii) Approximate $\tilde{p}_k$ as
$\hat{p}_k = \sum_{i=1}^{m} \alpha_i^{(l+1)} \mathcal{N}(X; \mu_i^{(l+1)}, \Sigma_i^{(l+1)})$

B. Error-Ellipse Resampling

We use a GCF for sequential Bayesian estimation in harsh environments, which is used to solve the non-Gaussian noise problem in a practical measurement model. However, based on the Bayesian recursive inference criterion, we can conclude that if *a priori* estimation is biased, the subsequent state estimation would also be affected. Therefore, we further analyze the geometric factors affecting the target node positioning accuracy, and then establish error-ellipse optimization. Finally, the EER algorithm is described as follows, which mainly realizes the rescreening of sampling points.

The error ellipse is often used in accuracy evaluation [35]. Let s indicate the uncertainty of state estimation, and then if a confidence probability β is given in advance, a confidence interval (s_1, s_2) could be found to satisfy

$$P(s_1 < s < s_2) = \beta. \tag{16}$$

In this article, the two-dimensional covariance matrix of N sampling points at time k is expressed as

$$R = \begin{bmatrix} \mathrm{cov}(x, x) & \mathrm{cov}(x, y) \\ \mathrm{cov}(y, x) & \mathrm{cov}(y, y) \end{bmatrix}. \tag{17}$$

If x is positively related to y, *vice versa*, then $\mathrm{cov}(x, y) = \mathrm{cov}(y, x)$. Therefore, the covariance matrix is always a symmetric one. When the center of error ellipse is not at the origin point, the equation could be expressed as

$$s = \frac{(x - x_p)^2}{\tau_1} + \frac{(y - y_p)^2}{\tau_2} \tag{18}$$

where τ_1 and τ_2 are, respectively, the largest and smallest eigenvector of the covariance matrix R. (x_p, y_p) is the estimated center position, and s is the scale of the error ellipse [15]. When the ellipse is tilted, the angle ε between the error-ellipse's major axis and the x-axis is expressed as

$$\varepsilon = \arctan \frac{\tau_1(y)}{\tau_1(x)} \tag{19}$$

Furthermore, assume the rotated coordinates are (x', y'), and then, the error-ellipse constraint represented by the rotated coordinates could be obtained as

$$s = \frac{\left((x' - x_p)\cos\varepsilon + (y' - y_p)\sin\varepsilon\right)^2}{\tau_1} + \frac{\left(-(x' - x_p)\sin\varepsilon + (y' - y_p)\cos\varepsilon\right)^2}{\tau_2} \tag{20}$$

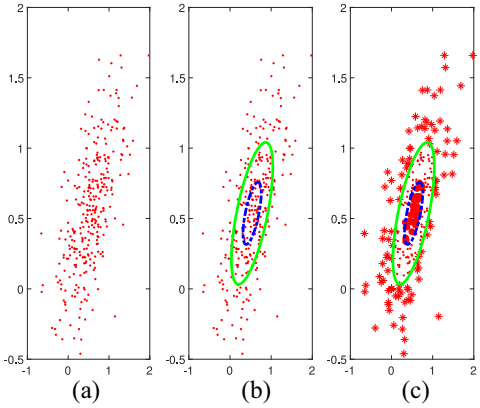

Fig. 5. Example of a resampled screening process. (a) Initial distribution of the sampling points. (b) Two different confidence level ellipse based on the covariance matrix of the sampling points. (c) Screening results for the sampling points of different levels.

p_0 is the prior distribution of initial status X_0. At the initial moment, the sampling points obey prior distribution p_0. Fig. 5 shows a resampling process based on error-ellipse estimation. In the resampling stage, two error ellipses are established according to the initial covariance matrix of N sampling points at time k, with different scales of 3σ (the outer one) and σ (the inner one), respectively. During the resampling, N sampling points are divided into three different levels on account of their geometric positions. N_a sampling points outside the outer ellipse are defined as insignificant ones, which would be discarded. The sampling points located in the middle of the two error ellipses would be retained. Then, the last N_b sampling points inside the inner ellipse are defined as significant ones, which would be replicated. Since we must ensure the number of overall sampling points remains unchanged, the first $N_c = N_a - \lfloor N_a/N_b \rfloor N_b$ significant sampling points would be replicated $c_1 = \lfloor N_a/N_b \rfloor + 2$ times, and then, the remaining $N_b - N_c$ ones are replicated $c_2 = \lfloor N_a/N_b \rfloor + 1$ times. Furthermore, the sampling points, which have performed the replication, would also be used as an initial input for the next iteration. The detailed description of the EER algorithm is shown in Algorithm 2.

C. GCF Based on EER

As mentioned above, GCF uses the Gaussian mixture distribution to approximate the posterior probability $\tilde{p}(X_k|Z_{1:k})$ and estimates the unknown parameters in the Gaussian mixture model with the Gaussian condensation theory. However, the Bayesian estimation could obtain the posterior probability density by *prediction* and *update*, recursively. The previously estimated deviation may affect the subsequent state estimation. On this basis, we propose a GCF based on the EER algorithm, which screens and replicates the sampling points in the

Algorithm 2 EER

Input: $[\{X_k^i\}_{i=1}^N\}, (x_p, y_p)] \leftarrow$ status, confidence center
Output: $\{\hat{X}_k^i\}_{i=1}^N \leftarrow$ status
for $i = 1, N$ **do**
  $d \leftarrow ellipse(X_k^i, (x_p, x_p)) \triangleright formula(20)$;
  if $d > s_1$ **then**
    $indexA(N_a) = i$;
    $N_a = N_a + 1$;
  else if $d < s_2$ **then**
    $indexB(N_b) = i$;
    $N_b = N_b + 1$;
  else
    $\hat{X}_k^{index(n)} = X_k^i$;
    $n = n + 1$;
  end if
end for
$N_c = N_a - \lfloor N_a/N_b \rfloor * N_b$;
for $j = 1, N_b$ **do**
  if $j \leq N_c$ **then**
    $c^{(j)} = \lfloor N_a/N_b \rfloor + 2$;
    for $l = 1, c^{(j)}$ **do**
      $\hat{X}_k^{index(n)} = X_k^{indexB(j)}$;
      $n = n + 1$;
    end for
  else
    $c^{(j)} = \lfloor N_a/N_b \rfloor + 1$;
    for $l = 1, c^{(j)}$ **do**
      $\hat{X}_k^{index(n)} = X_k^{indexB(j)}$;
      $n = n + 1$;
    end for
  end if
end for

Algorithm 3 EER-GCF

Input: $[X_0] \leftarrow$ initial status
Output: $\{\hat{X}_k\}_{k=1}^K \leftarrow$ status estimation
for $k = 0, K$ **do**
  if $k = 0$ **then**
    $X_0^{j=1:N} \sim \hat{p}_0 \leftarrow$is the prior distribution of X_0 and $\hat{p}_0 \sim \mathcal{N}(\mu_0, Q_0)$
  else
    for $j = 1, N$ **do**
      $X_k^j \leftarrow f_1(X_{k-1}^j) \Rightarrow$state transition function
    end for
    $\{\hat{X}_k^j\}_{j=1}^N \leftarrow EER(\{X_k^j\}_{j=1}^N\}, (x_p, y_p)) \triangleright$Algorithm 2: error-ellipse re-sampling
    $\mu_k^{(i)} = F_k \mu_{k-1}^{(i)}$
    $Q_k^{(i)} = F_k Q_{k-1}^{(i)} F_k^T + \gamma^2$
    $\tilde{p}(X_k|Z_{1:k-1}) = \sum_{i=1}^m \alpha_i \mathcal{N}(\{\hat{X}_k^j\}_{j=1}^N; \mu_k^{(i)}, Q_k^{(i)}) \triangleright formula(9)$
    $\tilde{p}_k \leftarrow \tilde{p}(X_k|Z_{1:k-1}) * f_2(Z_k) \Rightarrow$ likelihood function
    $\{\lambda_k, \hat{p}_k\} \leftarrow GCF(\tilde{p}_k) \triangleright$Algorithm 1: Gaussian condensation filter
    $\hat{X}_k = find(\hat{p}_k = max(\hat{p}_k))$
  end if
end for

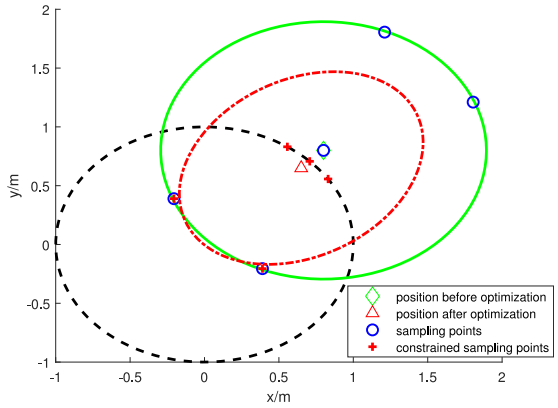

Fig. 6. Example of constrained sampling: ○ represents those nodes for resampling. The points within the constraint range (dotted circle) are remained. The points outside the distance constraint range are projected, and + indicates the sampling point after resampling. ◇ and △ are, respectively, the estimate before and after optimization.

prediction step on account of their geometric positions to the confidence center. Therefore, it can suppress the cumulative error in target tracking.

EER-GCF creates two ellipses with scales of 3σ and σ, respectively. To suppress the impact of previous estimation errors, it performs replicating, retaining, and discarding on sampling points at different levels, as discussed in the previous section. With this constrained resampling strategy, the posterior probability density $\tilde{p}$ could be obtained by recursive *prediction* and *update*. Considering that the sufficient statistic $\tilde{p}$ may infinitely increase in temporal series, the Gaussian condensation theory is used to approximate $\tilde{p}$ as Gaussian mixture distribution $\hat{p}$. Finally, the state corresponding to the maximum of $\hat{p}$ is the expected estimation at the current moment. The detailed description of the proposed EER-GCF is shown in Algorithm 3.

D. Constraint Optimization Based on Spatial Distance

In this section, we integrate the spatial distance measurements between target nodes to cooperative localization. In this article, constrained Bayesian optimization is used to promote target tracking accuracy. First, EER-GCF is applied at each time slot to calculate the mean and covariance of state estimation as the prior knowledge of Bayesian optimization. Then, distances between target nodes should be acquired and introduced into the optimization process as constraints. Furthermore, optimized mean and covariance of the posterior distribution are derived by convex combination to approximate the integral calculation. The effectiveness of resampling under distance constraint is displayed in Fig. 6.

1) Bayesian Constraint Optimization: During the dynamic estimation process, the sequential EER-GCF filter will output the initial positions of each target at time k. $\{A_{k,1}, A_{k,2}, \ldots, A_{k,M}\}$ works as the prior knowledge of further cooperative Bayesian optimization. Then, we define the joint state of the ith node and the jth node at time k as $r_k = [A_{k,i}, A_{k,j}]^T$. Therefore, the mean $u_k = [u_{k,i}, u_{k,j}]^T$ and covariance $C_k = [C_{k,i}, C_{k,j}]^T$ of the joint state could be obtained by GCF. Furthermore, given the distance constraint c, once the posterior probability density $p(r|c)$ is derived, the posterior mean $\hat{u}_{r|c}$ and covariance $\hat{C}_{r|c}$ of the target state could be obtained.

Assume that the ith target node can receive the measurement S_k of $M-1$ other target nodes at time k. The ith node

will select the values that satisfied the distance constraint $c : ||\rho r|| \leq S$, where $\rho = [I_2, -I_2]$, and I_k represents a k-degree identity matrix. We introduce a new state vector $z = Tr \in \mathbb{R}^4$, where r represents the joint state vector of the target node, and z is a Gaussian distribution with mean u_z and covariance C_z, i.e., $z \sim \mathcal{N}(u_z, C_z)$. Therein, $u_z = Tu_r$ and $C_z = TC_rT^T$ could be obtained. The state vector z is given by a reversible linear transformation, which consists of the subvector $z_1 = A_1 - A_2$ and $z_2 = A_1 + A_2$, where A_1 and A_2 represent arbitrary two nodes that can range with each other. Therefore, $T = \begin{bmatrix} I_2 & -I_2 \\ I_2 & I_2 \end{bmatrix}$ can be verified. After adding the distance constraint, we obtain new constraint information

$$c : \left\| \rho T^{-1} z \right\| = \|z_1\| \leq S. \tag{21}$$

Therefore, the distance constraint is only related to z_1.

2) Affine Transformation: We need to calculate the posterior mean $\hat{u}_{r|c}$ and covariance $\hat{C}_{r|c}$. As it is known that $\hat{u}_{r|c} = T^{-1}u_{z|c}$ and $\hat{C}_{r|c} = T^{-1}C_{z|c}T^{-T}$, we may turn the problem into finding $u_{z|c}$ and $C_{z|c}$. With the following affine transformation, we could obtain

$$\begin{aligned} u_{z_2|z_1} &= \upsilon_{z_2} + Bz_1 \\ C_{z_2|z_1} &= \upsilon_{z_2} - BC_{z_2z_1}^T. \end{aligned} \tag{22}$$

The intermediate variables in (22) are denoted as $B = C_{z_2z_1}C_{z_1}^{-1}$ and $\upsilon_{z_2} = u_{z_2} - Bu_{z_1}$, respectively. Let $u_{z_2|z_1} = [u_{z_1|c}, u_{z_2|c}]^T$. Then, the conditional mean $u_{z_1|c}$ of z_1 is expressed as

$$u_{z_1|c} = \int_{z_1} z_1 p(z_1|c) dz_1. \tag{23}$$

The conditional mean $u_{z_2|c}$ is expressed as

$$\begin{aligned} u_{z_2|c} &= \int_{z_1} \left[\int_{z_2} z_2 p(z_2|z_1) \right] p(z_1|c) dz_1 \\ &= \int_{z_1} u_{z_2|z_1} p(z_1|c) dz_1 = \int_{z_1} \left(\upsilon_{z_2} + Bz_1 \right) p(z_1|c) dz_1 \\ &= \upsilon_{z_2} + B \int_{z_1} z_1 p(z_1|c) dz_1 = \upsilon_{z_2} + Bu_{z_1|c}. \end{aligned} \tag{24}$$

The conditional covariance matrix $C_{z|c}$ is expressed as

$$C_{z|c} = D_{z|c} - u_{z|c}u_{z|c}^{\mathrm{T}} \tag{25}$$

where $D_{z|c} = \begin{bmatrix} D_{z_1|c} & D_{z_1z_2|c} \\ D_{z_1z_2|c} & D_{z_2|c} \end{bmatrix}$. Therefore, the covariance of posterior probability $p(z_1|c)$ can be expressed as

$$D_{z_1|c} = \int_{z_1} z_1 z_1^{\mathrm{T}} p(z_1|c) dz_1. \tag{26}$$

With the affine transformation, we could obtain the covariance

$$\begin{aligned} D_{z_1z_2|c} &= \int_{z_1} z_1 \left[\int_{z_2} z_2^T p(z_2|z_1) dz_2 \right] p(z_1|c) dz_1 \\ &= \int_{z_1} z_1 u_{z_2|z_1}^T p(z_1|c) dz_1 \\ &= u_{z_1|c}\upsilon_{z_2}^T + D_{z_1|c}B^T \end{aligned} \tag{27}$$

$$\begin{aligned} D_{z_2|c} &= \int_{z_1} \left[\int_{z_2} z_2 z_2^T p(z_2|z_1) dz_2 \right] p(z_1|c) dz_1 \\ &= \int_{z_1} D_{z_2|z_1} p(z_1|c) dz_1 \\ &= C_{z_2} - BC_{z_2z_1}^T + \upsilon_{z_2}\upsilon_{z_2}^{\mathrm{T}} + \upsilon_{z_2}u_{z_1|c}^T B^T \\ &\quad + Bu_{z_1|c}\upsilon_{z_2}^{\mathrm{T}} + BD_{z_1|c}B^T. \end{aligned} \tag{28}$$

Therefore, we only need to calculate the integral about $p(z_1|c)$ with (23) and (26). Then, the *posteriori* mean $u_{z_1|c}$ and covariance $C_{z_1|c}$ could be got by affine transformation without calculating $p(z|c)$ directly.

3) Integral Approximation: To avoid calculating complex numerical integration, we use a convex combination to approximate the conditional mean and covariance

$$\begin{aligned} \hat{u}_{z_1|c} &\simeq \sum_{i=0}^{2n} w^{(i)} z_1^{(i)} \\ \hat{D}_{z_1|c} &\simeq \sum_{i=0}^{2n} w^{(i)} z_1^{(i)} \left(z_1^{(i)} \right)^{\mathrm{T}} \end{aligned} \tag{29}$$

where $z_1^{(i)}$ and $w^{(i)}$ denote the sampling points and weights, respectively, and n is the dimensions of the state. When the probability mass β of the sampling point $z_1^{(i)}$ is within the constraint range, the approximate value remains unchanged. Otherwise, resample the points to ensure that the approximated average value falls within the convex boundary, thereby reducing the dispersion. Therefore, the parameter β determines whether the sampling point is valid. Use the following equation to select sampling points:

$$h^{(i)} = \begin{cases} u_{z_1} & i = 0 \\ u_{z_1} + s_\beta^{1/2} \left[C_{z_1}^{1/2} \right]_i & i = 1, \ldots, n \\ u_{z_1} - s_\beta^{1/2} \left[C_{z_1}^{1/2} \right]_i & i = n+1, \ldots, 2n \end{cases} \tag{30}$$

where S_β is the confidence scale that satisfies $¶(s \leq s_\beta) = \beta$ and $s = (z_1 - u_{z_1})^{\mathrm{T}} C_{z_1}^{-1} (z_1 - u_{z_1})$.

The deterministic sampling method will select $2n + 1$ sampling points, and the sampling points that do not satisfy the constraint conditions will be orthogonally projected to the constraint boundary. The following equation is used to sample:

$$z_1^{(i)} = \begin{cases} h^{(i)} & \text{if} \left\| h^{(i)} \right\| \leq S_k \\ \frac{S_k}{\|h^{(i)}\|} h^{(i)} & \text{others} \end{cases} \quad i = 0, \ldots, 2n. \tag{31}$$

The weight of the sampling point is updated as

$$w^i = \begin{cases} 1 - \frac{n}{s_\beta}, & i = 0 \\ \frac{1}{2s_\beta}, & i = 1, \ldots, 2n. \end{cases} \tag{32}$$

The estimated mean and covariance of the posterior can be obtained by the weighted average of the resampled sampling points $\{z_1^{(i)}\}_{i=0}^{2n}$. The description of the proposed constrained optimization based on spatial distance constraints is shown in Algorithm 4.

Algorithm 4 Constraint Optimization Based on Spatial Distance

Input: $\{u_r = [u_1, u_2]^T, C_r = [C_1, C_2]^T, S_{12}\} \leftarrow$ the mean of joint state and covariance, distance observation
Output: $\{\hat{u}_{r_1|c}, \hat{C}_{r_1|c}, \hat{u}_{r_2|c}, \hat{C}_{r_2|c}\} \leftarrow$ the mean and convariance of state after optimization
if $||u_1 - u_2|| \geqslant S_{12}$ **then**
  $u_z = Tu_r, C_z = TC_rT^T \leftarrow$reversible linear transformation
  $z_1 = A_1 - A_2, z_2 = A_1 + A_2$
  $s_\beta = P(\beta) \triangleright formula(16)$calculating a confidence scale
  $\begin{bmatrix} D_{z_1} & D_{z_1z_2} \\ D_{z_1z_2} & D_{z_2} \end{bmatrix} = D_z = C_z + u_z u_z^T$
  $C_{z_1} = D_{z_1|c} - u_{z_1}u_{z_1}^T, C_{z_2} = D_{z_2|c} - u_{z_2}u_{z_2}^T, C_{z_1z_2} = D_{z_1z_2|c} - u_{z_2}u_{z_1}^T$
  for $i = 0, 2n$ **do**
    $h^{(i)} \leftarrow sample(n = 2) \triangleright formula(30)$
    if $h^{(i)} > S_{12}$ **then**
      $z_1^{(i)} \leftarrow norm(h^{(i)}) \triangleright$ orthogonal projection
    else
      $z_1^{(i)} = h^{(i)}$
    end if
    if $i = 1$ **then**
      $w^{(i)} = 1 - n/s_\beta$
    else
      $w^{(i)} = 1 - 2/s_\beta$
    end if
  end for
  $B = C_{z_2z_1}C_{z_1}^{-1}, \upsilon_{z_2} = u_{z_1} - Bu_{z_1}$
  for $i = 0, 2n$ **do**
    $\hat{u}_{z_1|c} = \hat{u}_{z_1|c} + w^{(i)}z_1^{(i)}$
    $\hat{D}_{z_1|c} = \hat{D}_{z_1|c} + w^{(i)}z_1^{(i)}(z_1^{(i)})^T$
  end for
  $\hat{u}_{z_2|c} = \upsilon_{z_2} + Bu_{z_1|c} \triangleright formula(22)$
  $\hat{u}_{z|c} = [\hat{u}_{z_1|c}^T, \hat{u}_{z_2|c}^T]^T$
  $\hat{u}_{r|c} = T^{-1}\hat{u}_{z|c}$
  $\hat{D}_{z_1z_2|c} = u_{z_1|c}\upsilon_{z_2}^T + \hat{D}_{z_1|c}B^T \triangleright formula(27)$
  $\hat{D}_{z_2|c} = C_{z_2} - BC_{z_2z_1}^T + \upsilon_{z_2}\upsilon_{z_2}^T + \upsilon_{z_2}u_{z_1|c}^T\upsilon_{z_2}^T + B\hat{D}_{z_1|c}B^T \triangleright formula(28)$
  $C_{z|c} = D_{z|c} - u_{z|c}u_{z|c}^T \triangleright formula(25)$
  $\hat{C}_{r|c} = T^{-1}\hat{C}_{z|c}T^{-T}$
end if

E. CGCF Based on EER

This section first displayed a GCF based on EER to estimate each mobile node's position initially. Next, the target node obtains the information gain from the inertial data in a temporal sequence. Then, the spatial distance between target nodes is taken advantage of as mutual information to improve the tracking accuracy. Therefore, it can achieve a higher precision multitarget cooperative location.

When a GCF based on EER is applied, we first make a rough estimation of the target state according to the center point of a sampling set. Then, two error ellipses with different scales of 3σ and σ, respectively, are established, and we achieve a resampling algorithm by hierarchical screening. After obtaining the mutual information between the target nodes, the spatial distance constraint c is established.

$\hat{u}_{r|c}$, which is closer to the real position, is obtained based on constrained Bayesian optimization. Therefore, the position estimation $\hat{u}_{r|c}$ optimized by the spatial constraint is considered to update the center point (x_p, y_p). Furthermore, the filter estimation will obtain the spatial information gain of the previous time at the next moment. It can achieve cooperative localization based on the fusion of both temporal and spatial information. The description of the proposed cooperative EER-based GCF (CEER-GCF) is shown in Algorithm 5.

Algorithm 5 CEER-GCF

Input: $[X_0] \leftarrow$ initial status
Output: $\{\hat{u}_{r_1|c}\}_{k=1}^K \leftarrow$ status estimation
for $k = 0, K$ **do**
  if $k = 0$ **then**
    $X_0^{j=1:N} \sim \hat{p}_0 \leftarrow$is the prior distribution of X_0
  else
    for $j = 1, N$ **do**
      $X_k^j \leftarrow f_1(X_{k-1}^j) \Rightarrow$state transition function
    end for
    $\{\hat{X}_k^j\}_{j=1}^N \leftarrow EER(\{X_k^j\}_{j=1}^N\}, (x_p, y_p)) \triangleright$Algorithm 2: error-ellipse re-sampling
    $\mu_k^{(i)} = F_k\mu_{k-1}^{(i)}$
    $Q_k^{(i)} = F_kQ_{k-1}^{(i)}F_k^T + \gamma^2$
    $\tilde{p}(X_k|Z_{1:k-1}) = \sum_{i=1}^m \alpha_i\mathcal{N}(\{\hat{X}_k^j\}_{j=1}^N; \mu_k^{(i)}, Q_k^{(i)}) \triangleright formula(9)$
    $\tilde{p}_k \leftarrow \tilde{p}(X_k|Z_{1:k-1}) * f_2(Z_k) \Rightarrow$ likelihood function
    $\{\lambda_k, \hat{p}_k\} \leftarrow GCF(\tilde{p}_k) \triangleright$Algorithm 1: Gaussian condensation filter
    $\hat{X}_k = find(\hat{p}_k = max(\hat{p}_k))$
    $u_1 = \hat{X}_k, C_1 = \mathrm{cov}(\hat{X}_k^{1:N}) \leftarrow$ the mean and covariance of sampling points at time k
    $u_r = [u_1, u_2]^T, C_r = [C_1, C_2]^T \leftarrow$ the target node that satisfies spatial constraint
    $(\hat{u}_{r_1|c}, \hat{C}_{r_1|c}, \hat{u}_{r_2|c}, \hat{C}_{r_2|c}) \leftarrow CDS(u_r, C_r, S_{12}) \triangleright$ Algorithm 4: constraint optimization based on spatial distance
    $(x_p, y_p) \leftarrow f_1(\hat{u}_{r_1|c}) \leftarrow$ update the confidence center at time $k + 1$
  end if
end for

IV. Theoretical Analysis

In this section, we carry out the theoretical derivation to prove the validity of the proposed algorithm. First, PCRLB of multitarget cooperative tracking accuracy is derived. Next, the complexity analysis of both proposed and comparative methods is conducted.

A. Posterior Cramér–Rao Lower Bound

The PCRLB [36] provides the theoretical lower limit on the accuracy of our proposed algorithm. Define $\hat{X}_k$ as an unbiased estimate of the target state X_k. Thus, the mean-square error of the state estimate has the following form:

$$E\left\{\left(\hat{X}_k - X_k\right)\left(\hat{X}_k - X_k\right)^T\right\} \geq J_k^{-1} \tag{33}$$

where J_k is the Fisher information metric (FIM) at time k, and J_k^{-1} is PCRLB.

The multitarget cooperative tracking algorithm fuses spatial–temporal posterior information. Therefore, the joint PDF is redefined as

$$p\left(\hat{d}_k, \hat{l}_k, \hat{\theta}_k, \hat{X}_k\right) = p\left(\hat{d}_0|X_0\right)\prod_{i=1}^k p\left(\hat{d}_i|X_i\right)p\left(\hat{l}_k|X_{i-1}, X_i\right) \times p\left(\hat{\theta}_k|X_{i-1}, X_i\right) \tag{34}$$

where $\hat{d}_k$ is the estimated distance between the target nodes, and $\hat{l}_k$ and $\hat{\theta}_k$ denote the estimated step and estimated angle, respectively. Therefore, the joint probability density at time k is represented as

$$p_k = p\left(\hat{d}_{0:k}, \hat{l}_{0:k}, \hat{\theta}_{0:k}, \hat{X}_{0:k}\right) \tag{35}$$

Based on the joint PDF p_k, the Fisher information matrix for multitarget cooperative tracking is written as

$$\begin{aligned} J(X_{0:k}) &= \begin{bmatrix} E\left\{-\Delta_{X_{0:k-1}}^{X_{0:k-1}} \ln p_k\right\} & E\left\{-\Delta_{X_{0:k-1}}^{X_{0:k}} \ln p_k\right\} \\ E\left\{-\Delta_{X_{0:k}}^{X_{0:k-1}} \ln p_k\right\} & E\left\{-\Delta_{X_{0:k}}^{X_{0:k}} \ln p_k\right\} \end{bmatrix} \\ &= \begin{bmatrix} U_k & L_k \\ L_k^T & W_k \end{bmatrix}. \end{aligned} \tag{36}$$

According to [36], the Fisher information matrix J_k can be obtained by the pseudoinverse of the matrix $J(X_{0:k})$, namely

$$J_k = W_k - L_k^T U_k^{-1} L_k. \tag{37}$$

Furthermore, the joint PDF at time $k+1$ according to (34) and (35) is defined as

$$\begin{aligned} p_{k+1} = p_k p\left(\hat{d}_{k+1}|X_{k+1}\right) p\left(\hat{l}_{k+1}|X_k, X_{k+1}\right) \\ \cdot p\left(\hat{\theta}_{k+1}|X_k, X_{k+1}\right). \end{aligned} \tag{38}$$

The Fisher information matrix of multitarget cooperative tracking according to the joint PDF p_{k+1} can be expressed as

$$J(X_{0:k+1}) = \begin{bmatrix} U_k & L_k & 0 \\ L_k^T & W_k + H_k^{11} & H_k^{12} \\ 0 & H_k^{12} & \phi_{k+1} + H_k^{22} \end{bmatrix} \tag{39}$$

where H_k^{11}, H_k^{12}, and H_k^{22} stand for the posterior information based on inertial measurements, namely

$$\begin{aligned} H_k^{11} = E_{\hat{l},\hat{\theta}}\Big\{-\Delta_{X_k}^{X_k} \ln p\left(\hat{l}_{k+1}|X_k, X_{k+1}\right) \\ \cdot p\left(\hat{\theta}_{k+1}|X_k, X_{k+1}\right)\Big\} \end{aligned} \tag{40}$$

$$\begin{aligned} H_k^{12} = E_{\hat{l},\hat{\theta}}\Big\{-\Delta_{X_k}^{X_{k+1}} \ln p\left(\hat{l}_{k+1}|X_k, X_{k+1}\right) \\ \cdot \left(\hat{\theta}_{k+1}|X_k, X_{k+1}\right)\Big\} = \left(H_k^{21}\right)^T \end{aligned} \tag{41}$$

$$\begin{aligned} H_k^{22} = E_{\hat{l},\hat{\theta}}\Big\{-\Delta_{X_{k+1}}^{X_{k+1}} \ln p\left(\hat{l}_{k+1}|X_k, X_{k+1}\right) \\ \cdot p\left(\hat{\theta}_{k+1}|X_k, X_{k+1}\right)\Big\} \end{aligned} \tag{42}$$

where ϕ_{k+1} is the positional information based on range measurements at time $k+1$, namely

$$\phi_{k+1} = E_{\hat{d}_{k+1}}\left\{-\Delta_{X_{k+1}}^{X_{k+1}} \ln p\left(\hat{d}_{k+1}|X_{k+1}\right)\right\}. \tag{43}$$

Finally, the Fisher information matrix at time $k+1$ can be derived from $J(X_{0:k+1})$ and J_k, namely

$$\begin{aligned} J_{k+1} &= \phi_{k+1} + H_k^{22} - \begin{bmatrix} 0 & H_k^{21} \end{bmatrix} \begin{bmatrix} U_k & V_k \\ V_k^T & W_k + H_k^{11} \end{bmatrix} \begin{bmatrix} 0 \\ H_k^{12} \end{bmatrix} \\ &= \phi_{k+1} + H_k^{22} - H_k^{21}\left(J_k + H_k^{11}\right)^{-1} H_k^{12} \end{aligned} \tag{44}$$

where $H_k^{11} \neq H_k^{12} \neq H_k^{22}$ as the step noise and angle noise are non-Gaussian.

TABLE I
COMPLEXITY COMPARISON AMONG DIFFERENT ALGORITHMS

Algorithm	Complexity
UKF	$O(n*(2n+1))$
PF	$O(N*n)$
GCF	$O(m*n)$
EER-GCF	$O(m*n+N)$
CGCF	$O(M*r+m*n)$
CEER-GCF	$O(M*r+m*n+N)$

B. Complexity Analysis

Regarding the theoretical analysis, the complexity of nonlinear filter algorithms is directly related to the state dimension n. The UKF algorithm selects $2n+1$ sigma points, and the complexity of the UKF algorithm is $O(n*(2n+1))$. The complexity of the PF algorithm is directly affected by the number of particles and resampling, so the complexity of the PF algorithm is $O(N*n)$, where N is the number of particles. The GCF algorithm approximates the posterior probability distribution to a Gaussian mixture distribution, so the complexity of the GCF algorithm is $O(m*n)$, where m is the number of mixed Gaussian kernels. It is known that the number of particles N is typically several orders of magnitude larger than m to achieve adequate performance. Therefore, for high-dimensional problems, high complexity is usually inevitable.

For error-ellipse constraints, N sampling points need to be selected and replicated. If the original sampling points are all selected, and none need to be copied. The complexity of the resampling algorithm is $O(N)$. If each sampling point needs to be copied, and the maximum number of replications is no more than 2. Hence, the complexity of the resampling algorithm is $O(2N)$. In general, since the number of sampling points before and after resampling is unchanged, the number of sampling points within the inner ellipse will not exceed $N/3$, and the maximum number of replications will not exceed 2. Therefore, the complexity of the resampling algorithm is $O(N)$, and the complexity of EER-GCF is $O(m*n+N)$.

For cooperative algorithms, the complexity is related to the number of target nodes M in the cooperative network. The spatial distance constraint optimization algorithm is determined by sigma point sampling, and the complexity of the cooperative algorithm is directly related to the joint state vector dimension r. Therefore, the complexity of the CGCF algorithm is $O(M*r+m*n)$, and that of CEER-GCF is $O(M*r+m*n+N)$. Complexity comparisons among different algorithms are shown in Table I.

V. EXPERIMENTAL RESULTS AND ANALYSIS

A. Experiment Environment

We carried out the location tracking experiment of the target node by MATLAB. The simulation runs on a PC with Windows 10 operating system, Intel 4-core i5 CPU, and 16-GB memory. As the motion law of the mobile node conforms to the dynamic random walking process, the moving scene of the target node is set to 50 m × 50 m. The initial position

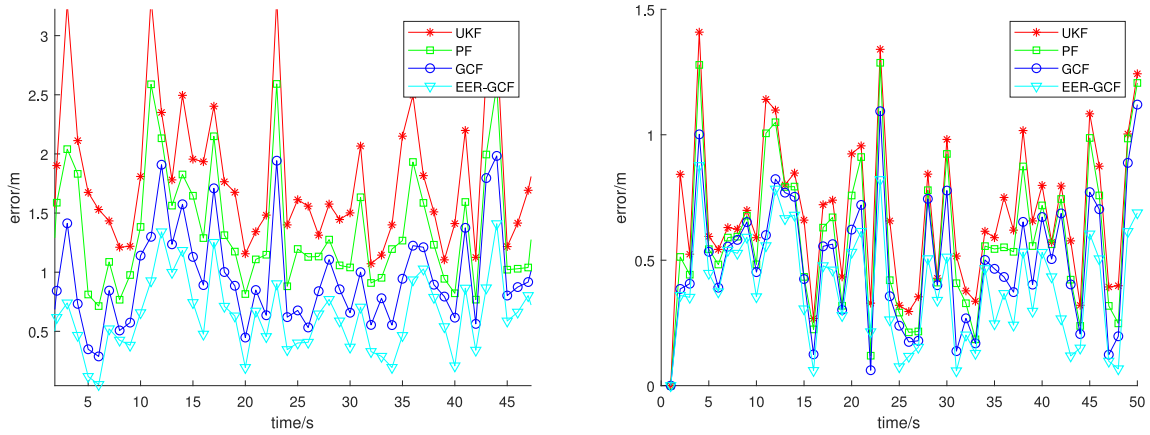

Fig. 7. Error distribution of different algorithms in single-target tracking. (a) Noise distribution obeys Student-t distribution. (b) Noise distribution obeys α-stable distribution.

TABLE II
PARAMETER SETTING

Parameter	Value
Sampling interval Δt	1(s)
Dynamic noise υ_k	1(m^2)
Velocity V	2(m/s)
Step noise $\eta_{1,k}$	0.1(m^2)
Angle noise $\eta_{2,k}$	5($^\circ$)
Measurement noise $\eta_{3,k}$	0.5(m^2)
Number of sample points N	4000

(x_0, y_0) and the heading angle θ of the target node are random in each experiment. It takes 50 steps randomly in the above-mentioned two-dimensional scene. In this article, the number of components for filters using mixtures of Gaussian is set as $m = 8$ [37]. The parameter settings in the experiment are detailed in Table II.

B. Performance Analysis of Single-Target Tracking

In harsh environments, the measurement model is often nonlinear, so it is difficult for single-target tracking algorithms to provide high-precision position estimation. This article proposes a GCF based on the EER algorithm to effectively estimate the state. In order to verify the effectiveness of EER-GCF, we compared it with state-of-the-art method, namely, UKF [13] and PF [15]. The error criterion is represented as the Euclidean distance between the forecast location (x_f, y_f) and the true location $(x_{\text{true}}, y_{\text{true}})$, namely

$$e = \sqrt{\left(x_f - x_{\text{true}}\right)^2 + \left(y_f - y_{\text{true}}.\right)^2} \tag{45}$$

To analyze how various noise distributions impact the performance, numerical experiments are performed, and the positioning error of a typical use case is shown in Fig. 7. The step noise $n_{1,k}$ and the angle noise $n_{2,k}$ obey the Student-t distribution [24]–[26] and α-stable distribution [23], respectively. Then, the following conclusions could be drawn.

1) Both UKF and PF have a large oscillation phenomenon, while GCF is more stable and has higher positioning precision. It shows that GCF-like filters have the advantage of improving the positioning accuracy in processing nonlinear measurement models.
2) Compared with GCF, EER-GCF has a smaller error distribution. As the iteration progresses, EER-GCF suppresses the effect of previous errors to a certain extent. This proves that the proposed EER-GCF algorithm can effectively improve the accuracy of single-target tracking.
3) When the measurement noise fits for various distributions, compared with other methods, EER-GCF can always maintain a relatively high accuracy, which verifies that our proposed algorithm can, to some extent, conquer the problem of non-Gaussian noise.

Furthermore, to verify the stability of EER-GCF, a random-walking-based experiment is performed, where UKF, PF, and GCF are also considered as contrast methods. They performed the random walk $K = 100$ times, and the root mean-square error is defined as

$$\text{RMSE} = \sqrt{\frac{1}{K}\sum_{i=1}^{k} e^2}. \tag{46}$$

Fig. 8 shows the root mean-square error of different algorithms in single-target tracking. The following conclusions could be drawn. The performance of UKF is relatively poor. PF and GCF have a closer root mean-square error distribution, but GCF still outperforms on precision. The error curve of EER-GCF is significantly lower than the others. Compared with GCF, the accuracy of EER-GCF is improved by 28.6%, and it has obvious advantages in estimation accuracy and stability.

The cumulative distribution function (CDF) of RMSE in single-target tracking is shown in Fig. 9. The positioning error of EER-GCF is less than 1 m with 97% probability, and that of GCF is less than 1.4 m with the same probability. It also verifies the effectiveness of EER-GCF in single-target tracking.

Then, the impact of noise variance on the positioning performance will be discussed. By setting different noise covariances, EER-GCF and contrast algorithms are implemented

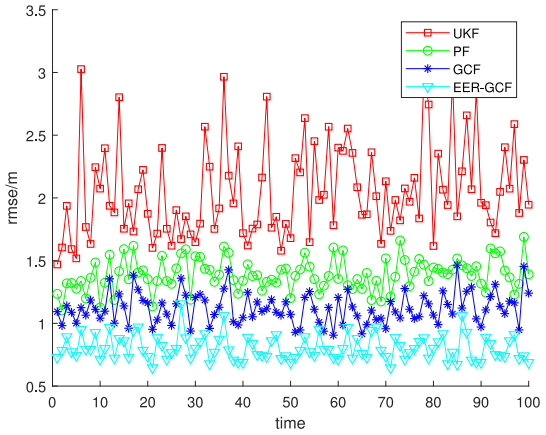

Fig. 8. RMSE of different algorithms in single-target tracking.

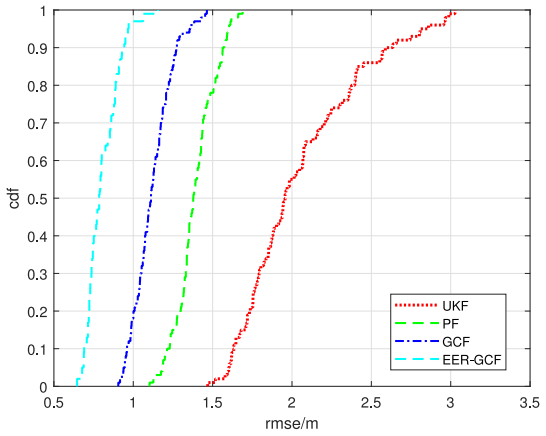

Fig. 9. CDF of different algorithms' RMSE in single-target tracking.

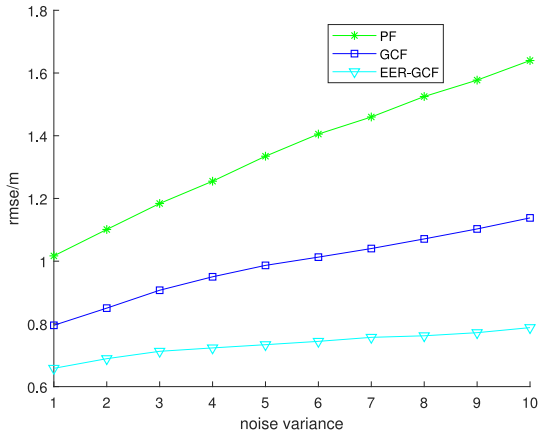

Fig. 10. Influence of noise variance on tracking accuracy.

to take 100 steps random walk. The detailed results are shown in Fig. 10. It can be seen from the figure that the tracking error grows with the increase of noise variance. EER-GCF has higher precision than the others, and it is less affected by the noise variance.

To analyze how the number of sampling points impacts the tracking performance, experiments are set up using GCF and EER-GCF. The precision is represented by RMSE. In addition, algorithms' execution time is also taken into consideration,

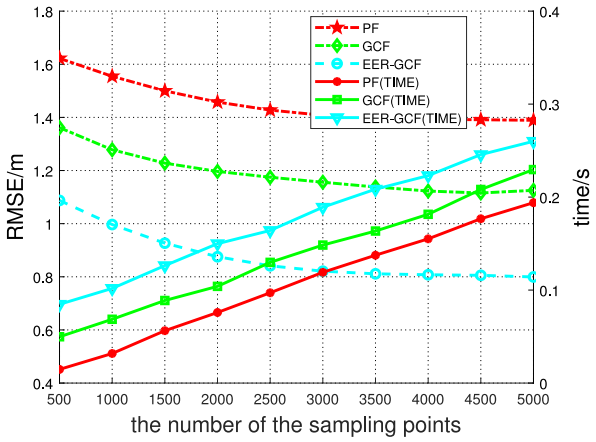

Fig. 11. Influence of the number of sampling points on tracking accuracy.

which can, to some extent, verify the complexity of various algorithms. The detailed results are shown in Fig. 11, from which the following conclusions could be obtained: as the number of sampling points increases, the positioning error gradually decreases, and finally, tend to converge. However, the runtime increases linearly. When the sampling points' number is less than 4000, as it increases, the accuracy improves significantly. While it is greater than 4000 and generally increases, the positioning error changes more smoothly. Therefore, to balance the marginal cost of accuracy and execution, an appropriate number of sampling points should be selected, and 4000 is preferred in this article.

C. Performance Analysis of Multitarget Cooperative Tracking

Our proposed multitarget cooperative tracking algorithm, i.e., CEER-GCF, integrates spatial distance information to obtain high precision, aiming to suppress the cumulative error problem caused by a nonlinear measurement model. In order to verify its effectiveness, the random walking experiments were repeated 100 times with considering cooperative PF (CPF) [15], CGCF, and CEER-GCF. The cooperative root mean-square error is considered as assessment criteria, which is defined as

$$\text{CRMSE} = \frac{1}{M}\sum_{i=1}^{M}\sqrt{\frac{1}{K}\sum_{j=1}^{k} e^2}. \tag{47}$$

Furthermore, the statistical positioning errors of all-mentioned algorithms are compared with PCRLB [36] under the same noise condition. The results are shown in Fig. 12, where the following conclusions could be drawn:

1) The cooperative root mean-square error curves of all mentioned cooperative algorithms are stable in general. The suitable method could effectively fuse the information of multiple single targets and utilize it comprehensively to achieve performance optimization. Namely, cooperative algorithms have higher stability.
2) The positioning accuracy of CPF reaches 0.39 m, while that of CGCF is 0.32 m, and that of CEER-CGCF

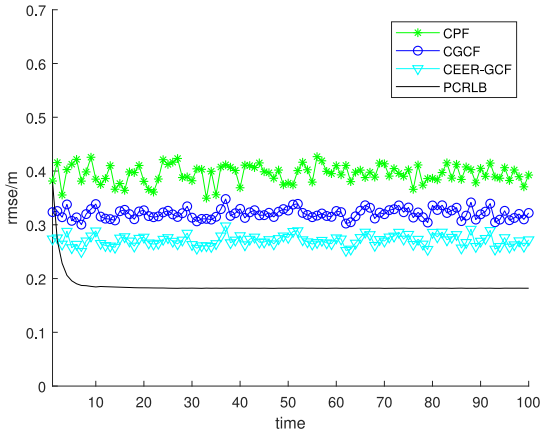

Fig. 12. RMSE of different algorithms in multitarget tracking.

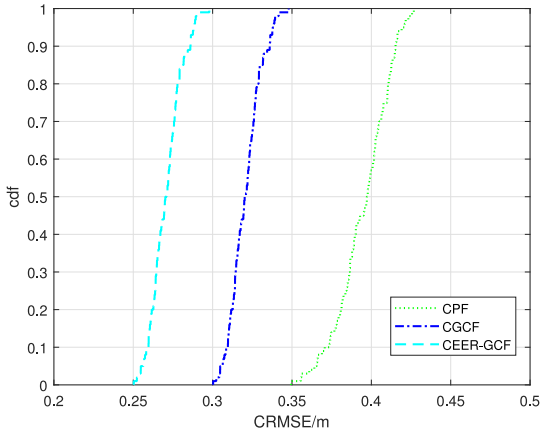

Fig. 13. CDF of different algorithms' RMSE in multitarget tracking.

reaches 0.27 m. CEER-GCF has higher accuracy, and the root mean-square error curve of CEER-GCF is closer to the cooperative PCRLB. It verifies the effectiveness of our proposed algorithm described in this article in cooperative tracking.

Fig. 13 shows the CDF curve of the root mean-square error of different algorithms in multitarget tracking. We can conclude that the positioning accuracy of CPF is less than 0.45 m, the positioning accuracy of CGCF is less than 0.35 m, and the positioning accuracy of CEER-GCF is less than 0.3 m. It also verifies that the CEER-GCF algorithm proposed in this article can achieve higher precision cooperative tracking.

Fig. 14 shows how the number of target nodes impacts the performance of different cooperative tracking algorithms, from which we can conclude the following.

1) With the increase of the number of targets, the positioning error curve is smooth, and CEER-GCF is more accurate. Therefore, when the larger the number of targets is, the algorithm described in this article is more effective, which is quite suitable for applications with large-scale deployment.
2) With the increase of the number of targets, the execution time of all algorithms gradually grows, and that of CEER-GCF is slightly higher than other algorithms.

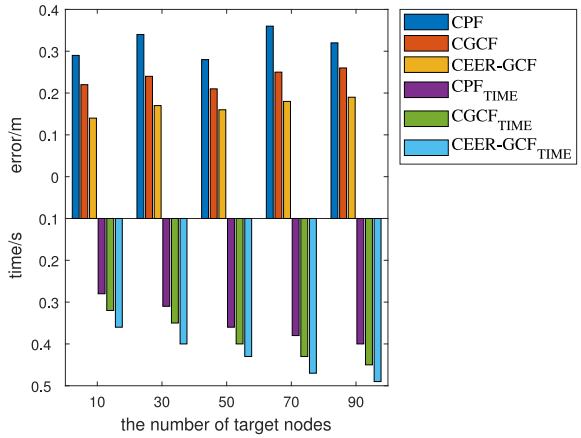

Fig. 14. Influence of the number of target nodes on the performance of the algorithm.

TABLE III
POSITIONING ACCURACY OF DIFFERENT ALGORITHMS

Method	max-Error (m)	min-Error (m)	avg-Error (m)	Time (s)
UKF	3.02	1.47	2.05	**0.06**
PF	1.69	1.10	1.39	0.15
GCF	1.46	0.91	1.12	0.18
EER-GCF	**1.16**	**0.64**	**0.80**	0.22
CPF	0.43	0.35	0.39	**0.19**
CGCF	0.35	0.30	0.32	0.22
CEER-GCF	**0.29**	**0.25**	**0.27**	0.26

However, it can satisfy the real-time requirements of general systems.

To sum up, as shown in Table III, we can conclude the following.

1) In single-target tracking, GCF can reach a positioning accuracy of about 1.12 m. Compared with other algorithms, GCF has higher accuracy, but its running time is slightly higher. This is due to the iterative solution of the GCF in the Gaussian condensation step.
2) EER-GCF can reach a positioning accuracy of about 0.80 m in single-target tracking and provides a higher positioning accuracy. Since the resampling algorithm needs replicating, the execution of EER-GCF runs slightly longer. However, it is completely acceptable for real-time applications.
3) In the multitarget tracking, CEER-GCF can achieve a positioning accuracy of about 0.27 m. Compared with single-target tracking, CEER-GCF greatly improves the positioning accuracy and stability. A cooperative tracking algorithm takes time to optimize spatial information, but it can satisfy the real-time requirements of most systems.

VI. CONCLUSION

In this article, a GCF is proposed to conquer non-Gaussian noise in target tracking. In the Gaussian condensation stage, the unknown parameters in the Gaussian mixture model are adjusted by recursive iteration, and the model is used to

approximate the true posterior probability distribution. In the experiment, a single target tracking simulation was performed based on the random walking process. GCF outperforms other nonlinear filters and shows its ability to conquer non-Gaussian noise.

An EER-GCF is proposed to suppress the cumulative errors of inertial target tracking. According to the sampling points' geometrical positions, we realized the hierarchical screening of the sampling points. The experimental results verify that EER-GCF can effectively suppress the influence of cumulative errors.

For cooperative tracking scenes, a constrained GCF (CEER-GCF) is proposed. We took the information gain in temporal series as the prior knowledge of spatial cooperative optimization and established the distance constraint between target nodes. Then, we obtained the state optimization based on spatial distance constraints. The results verify that the CEER-GCF algorithm can achieve high-precision positioning in harsh environments.

APPENDIX

Parameterize the Gaussian mixture model with $(\varsigma_1, \ldots, \varsigma_m, \ldots, \mu_1, \ldots, \mu_m, \sum_1^{-1}, \ldots, \sum_m^{-1})$, where

$$\alpha_i = \frac{e^{-\varsigma_i}}{\sum_{j=1}^{m} e^{-\varsigma_i}}$$

λ^* is a stationary point of $\Phi(\lambda)$ if and only $(\partial\Phi/\partial\varsigma_i)(\lambda^*)$, $(\partial\Phi/\partial\mu_i)(\lambda^*)$, and $[\partial\Phi/(\partial\sum_i^{-1})](\lambda^*)$ vanish for $i = 1, \ldots, m$. Using the properties $(\partial\Phi/\partial X)(X^TLX) = X^T(L+L^T)$, $(\partial\Phi/\partial L)(X^TLX) = XX^T$, and $(\partial\Phi/\partial L)(\log|L|) = L^{-1}$ for any $X \in \mathbb{R}^{\ltimes}$ and symmetric matrix L, it is straightforward to show that

$$\frac{\partial\Phi}{\partial\varsigma_i} = -\alpha_i + E_p\left\{\frac{q_i(X;\lambda)}{q(X;\lambda)}\right\}$$

$$\frac{\partial\Phi}{\partial\mu_i} = -E_p\left\{\frac{q_i(X;\lambda)(X-\mu_i)^T\sum_i^{-1}}{q(X;\lambda)}\right\}$$

$$\frac{\partial\Phi}{\partial\sum_i^{-1}} = -\frac{1}{2}E_p\left\{\frac{q_i(X;\lambda)\left(\sum_i -(X-\mu_i)(X-\mu_i)^T\right)}{q(X;\lambda)}\right\}$$

and the result is obtained by checking that these partial derivatives vanish at λ^*.

REFERENCES

[1] C. Chen, P. Zhao, C. X. Lu, W. Wang, A. Markham, and N. Trigoni, "Deep-learning-based pedestrian inertial navigation: Methods, data set, and on-device inference," *IEEE Internet Things J.*, vol. 7, no. 5, pp. 4431–4441, May 2020. [Online]. Available: http://dx.doi.org/10.1109/JIOT.2020.2966773

[2] Z. Kashino, G. Nejat, and B. Benhabib, "A hybrid strategy for target search using static and mobile sensors," *IEEE Trans. Cybern.*, vol. 50, no. 2, pp. 856–868, Feb. 2020. [Online]. Available: http://dx.doi.org/10.1109/TCYB.2018.2875625

[3] K. Ansari, "Cooperative position prediction: Beyond vehicle-to-vehicle relative positioning," *IEEE Trans. Intell. Transp. Syst.*, vol. 21, no. 3, pp. 1121–1130, Mar. 2020. [Online]. Available: http://dx.doi.org/10.1109/TITS.2019.2902572

[4] C. Xu, M. Ji, Y. Qi, and X. Zhou, "MCC-CKF: A distance constrained Kalman filter method for indoor TOA localization applications," *Electronics*, vol. 8, no. 5, p. 478, 2019. [Online]. Available: http://dx.doi.org/10.3390/electronics8050478

[5] X. Niu, Y. Li, J. Kuang, and P. Zhang, "Data fusion of dual foot-mounted IMU for pedestrian navigation," *IEEE Sensors J.*, vol. 19, no. 12, pp. 4577–4584, Jun. 2019.

[6] H. Ahmed and M. Tahir, "Improving the accuracy of human body orientation estimation with wearable IMU sensors," *IEEE Trans. Instrum. Meas.*, vol. 66, no. 3, pp. 535–542, Mar. 2017.

[7] C. Xu, X. Wang, S. Duan, and J. Wan, "Spatial-temporal constrained particle filter for cooperative target tracking," *J. Netw. Comput. Appl.*, vol. 176, Feb. 2021, Art. no. 102913. [Online]. Available: http://dx.doi.org/10.1016/j.jnca.2020.102913

[8] S. Zihajehzadeh and E. J. Park, "A novel biomechanical model-aided IMU/UWB fusion for magnetometer-free lower body motion capture," *IEEE Trans. Syst., Man, Cybern., Syst.*, vol. 47, no. 6, pp. 927–938, Jun. 2017.

[9] C. Xu, J. He, X. Zhang, C. Yao, and P.-H. Tseng, "Geometrical kinematic modeling on human motion using method of multi-sensor fusion," *Inf. Fusion*, vol. 41, pp. 243–254, May 2018. [Online]. Available: http://dx.doi.org/10.1016/j.inffus.2017.09.014

[10] J. Qiu *et al.*, Centralized fusion based on interacting multiple model and adaptive Kalman filter for target tracking in underwater acoustic sensor networks," *IEEE Access*, vol. 7, pp. 25948–25958, 2019. [Online]. Available: http://dx.doi.org/10.1109/access.2019.2899012

[11] A. Baghdadi, L. A. Cavuoto, and J. L. Crassidis, "Hip and trunk kinematics estimation in gait through Kalman filter using IMU data at the ankle," *IEEE Sensors J.*, vol. 18, no. 10, pp. 4253–4260, May 2018.

[12] M. Ghobadi, P. Singla, and E. T. Esfahani, "Robust attitude estimation from uncertain observations of inertial sensors using covariance inflated multiplicative extended Kalman filter," *IEEE Trans. Instrum. Meas.*, vol. 67, no. 1, pp. 209–217, Jan. 2018.

[13] W. You, F. Li, L. Liao, and M. Huang, "Data fusion of UWB and IMU based on unscented Kalman filter for indoor localization of quadrotor UAV," *IEEE Access*, vol. 8, pp. 64971–64981, 2020.

[14] C. Xu, J. He, Y. Li, X. Zhang, X. Zhou, and S. Duan, "Optimal estimation and fundamental limits for target localization using IMU/TOA fusion method," *IEEE Access*, vol. 7, pp. 28124–28136, 2019. [Online]. Available: http://dx.doi.org/10.1109/ACCESS.2019.2902127

[15] X. Wang, C. Xu, S. Duan, and J. Wan, "Error-ellipse-resampling-based particle filtering algorithm for target tracking," *IEEE Sensors J.*, vol. 20, no. 10, pp. 5389–5397, May 2020.

[16] D. Feng, C. Wang, C. He, Y. Zhuang, and X.-G. Xia, "Kalman-filter-based integration of IMU and UWB for high-accuracy indoor positioning and navigation," *IEEE Internet Things J.*, vol. 7, no. 4, pp. 3133–3146, Apr. 2020. [Online]. Available: http://dx.doi.org/10.1109/JIOT.2020.2965115

[17] Q. Li, B. Chen, and M. Yang, "Improved two-step constrained total least-squares TDOA localization algorithm based on the alternating direction method of multipliers," *IEEE Sensors J.*, vol. 20, no. 22, pp. 13666–13673, Nov. 2020. [Online]. Available: http://dx.doi.org/10.1109/JSEN.2020.3004235

[18] C. Xu, J. He, X. Zhang, P.-H. Tseng, and S. Duan, "Toward near-ground localization: Modeling and applications for TOA ranging error," *IEEE Trans. Antennas Propag.*, vol. 65, no. 10, pp. 5658–5662, Oct. 2017. [Online]. Available: http://dx.doi.org/10.1109/TAP.2017.2742551

[19] N. A. Alsindi, B. Alavi, and K. Pahlavan, "Measurement and modeling of ultrawideband TOA-based ranging in indoor multipath environments," *IEEE Trans. Veh. Technol.*, vol. 58, no. 3, pp. 1046–1058, Mar. 2009. [Online]. Available: http://dx.doi.org/10.1109/TVT.2008.926071

[20] P. Wang, J. He, L. Xu, Y. Wu, C. Xu, and X. Zhang, "Characteristic modeling of TOA ranging error in rotating anchor-based relative positioning," *IEEE Sensors J.*, vol. 17, no. 23, pp. 7945–7953, Dec. 2017. [Online]. Available: http://dx.doi.org/10.1109/JSEN.2017.2757700

[21] S. Li, M. Hedley, I. B. Collings, and M. Johnson, "Integration of IMU in indoor positioning systems with non-Gaussian ranging error distributions," in *Proc. IEEE/ION Position Location Navig. Symp. (PLANS)*, Savannah, GA, USA, 2016, pp. 577–583. [Online]. Available: http://dx.doi.org/10.1109/PLANS.2016.7479748

[22] M. L. Hoang, S. D. Iacono, V. Paciello, and A. Pietrosanto, "Measurement optimization for orientation tracking based on no motion no integration technique," *IEEE Trans. Instrum. Meas.*, vol. 70, pp. 1–10, 2021. [Online]. Available: http://dx.doi.org/10.1109/TIM.2020.3035571

[23] A. Song, Z. Tong, and T. Qiu, "A new correntropy based TDE method under α-stable distribution noise environment," *J. Electron.*, vol. 28, pp. 284–288, Dec. 2011.

[24] H. Zhu, H. Leung, and Z. He, "A variational Bayesian approach to robust sensor fusion based on student-*t* distribution," *Inf. Sci.*, vol. 221, pp. 201–214, Feb. 2013.

[25] C. R. B. Cabral, V. H. Lachos, and C. B. Zeller, "Multivariate measurement error models using finite mixtures of skew-student t distributions," *J. Multivariate Anal.*, vol. 124, pp. 179–198, Feb. 2014.
[26] M. J. Salois and K. G. Balcombe, "A generalized Bayesian instrumental variable approach under student t-distributed errors with application," *Manchester School*, vol. 83, no. 5, pp. 499–522, 2015.
[27] T. Li, M. Bolic, and P. M. Djuric, "Resampling methods for particle filtering: Classification, implementation, and strategies," *IEEE Signal Process. Mag.*, vol. 32, no. 3, pp. 70–86, May 2015.
[28] J. L. C. Villacrés, Z. Zhao, T. Braun, and Z. Li, "A particle filter-based reinforcement learning approach for reliable wireless indoor positioning," *IEEE J. Sel. Areas Commun.*, vol. 37, no. 11, pp. 2457–2473, Nov. 2019. [Online]. Available: http://dx.doi.org/10.1109/JSAC.2019.2933886
[29] H. Cao, P. Zhang, T. Lu, H. Gu, and N. Gu, "Real-time user activity recognition modeling method based on sensor distance," *Comput. Eng.*, vol. 45, no. 2, pp. 1–6, 2019.
[30] J.-O. Nilsson, D. Zachariah, I. Skog, and P. Händel, "Cooperative localization by dual foot-mounted inertial sensors and inter-agent ranging," *EURASIP J. Adv. Signal Process.*, vol. 2013, p. 164, Oct. 2013.
[31] Z. Wang, H. Zhang, T. Lu, and T. A. Gulliver, "Cooperative RSS-based localization in wireless sensor networks using relative error estimation and semidefinite programming," *IEEE Trans. Veh. Technol.*, vol. 68, no. 1, pp. 483–497, Jan. 2019. [Online]. Available: http://dx.doi.org/10.1109/TVT.2018.2880991
[32] X. R. Li and V. P. Jilkov, "Survey of maneuvering target tracking. Part I. Dynamic models," *IEEE Trans. Aerosp. Electron. Syst.*, vol. 39, no. 4, pp. 1333–1364, Oct. 2003. [Online]. Available: http://dx.doi.org/10.1109/taes.2003.1261132
[33] S. Mehryar, P. Malekzadeh, S. Mazuelas, P. Spachos, K. N. Plataniotis, and A. Mohammadi, "Belief condensation filtering for RSSI-based state estimation in indoor localization," in *Proc. IEEE Int. Conf. Acoust. Speech Signal Process. (ICASSP)*, Brighton, U.K., 2019, pp. 8385–8389. [Online]. Available: http://dx.doi.org/10.1109/ICASSP.2019.8683560
[34] K. L. Anderson and R. A. Iltis, "A distributed bearings-only tracking algorithm using reduced sufficient statistics," *IEEE Trans. Aerosp. Electron. Syst.*, vol. 32, no. 1, pp. 339–349, Jan. 1996. [Online]. Available: http://dx.doi.org/10.1109/7.481273
[35] H. Ghanbari, S. Homayouni, P. Ghamisi, and A. Safari, "Radiometric normalization of multitemporal and multisensor remote sensing images based on a Gaussian mixture model and error ellipse," *IEEE J. Sel. Topics Appl. Earth Observ. Remote Sens.*, vol. 11, no. 11, pp. 4526–4533, Nov. 2018. [Online]. Available: http://dx.doi.org/10.1109/JSTARS.2018.2871373
[36] M. Z. Win, Y. Shen, and W. Dai, "A theoretical foundation of network localization and navigation," *Proc. IEEE*, vol. 106, no. 7, pp. 1136–1165, Jul. 2018.
[37] J. H. Kotecha and P. M. Djuric, "Gaussian sum particle filtering," *IEEE Trans. Signal Process.*, vol. 51, no. 10, pp. 2602–2612, Oct. 2003.

Cheng Xu (Member, IEEE) received the B.E., M.S., and Ph.D. degrees from the University of Science and Technology Beijing (USTB), Beijing, China, in 2012, 2015, and 2019, respectively.

He is currently working as an Associate Professor with the Data and Cyber-Physical System Lab, USTB. He was supported by the Postdoctoral Innovative Talent Support Program from Chinese government in 2019.

Dr. Xu is an Associate Editor of *International Journal of Wireless Information Networks*. His research interests now include swarm intelligence, multirobots network, wireless localization, and Internet of Things.

Hang Wu is currently pursuing the master's degree with the University of Science and Technology Beijing, Beijing, China.

Her research interests include wireless indoor positioning, patter recognition, and Internet of Things.

Shihong Duan received the Ph.D. degree in computer science from the University of Science and Technology Beijing (USTB), Beijing, China.

She is an Associate Professor with the School of Computer and Communication Engineering, USTB. Her research interests include wireless indoor positioning, multirobots network, and Internet of Things.